Published in final edited form as:

Neuroimage. 2015 May 1; 111: 179–185. doi:10.1016/j.neuroimage.2015.02.017.

Perigenual anterior cingulate event-related potential precedes stop signal errors

Andrew Chang[a], **Chien-Chung Chen**[a,b,*], **Hsin-Hung Li**[a], and **Chiang-Shan R. Li**[c,d,e,**]

[a]Department of Psychology, National Taiwan University, Taipei 106, Taiwan

[b]Center for Neurobiology and Cognitive Science, National Taiwan University, Taipei 106, Taiwan

[c]Department of Psychiatry, Yale University, New Haven, CT 06511, USA

[d]Department of Neurobiology, Yale University, New Haven, CT 06511, USA

[e]Interdepartmental Neuroscience Program, Yale University, New Haven, CT 06511, USA

Abstract

Momentary lapses in attention disrupt goal-directed behavior. Attentional lapse has been associated with increased "default-mode" network (DMN) activity. In our previous fMRI study of a stop signal task (SST), greater activation of the perigenual anterior cingulate cortex (pgACC) – an important node of the DMN – predicts stop signal errors. In event-related potential (ERP) studies, the amplitude of an error-preceding positivity (EPP) also predicts response error. However, it is not clear whether the EPP originates from DMN regions. Here, we combined high-density array EEG and an SST to examine response-locked ERPs of error preceding trials in twenty young adult participants. The results showed an EPP in go trials that preceded stop error than stop success trials. Importantly, source modeling identified the origin of the EPP in the pgACC. By employing a bootstrapping procedure, we further confirmed that pgACC rather than the dorsal ACC as the source provides a better fit to the EPP. Together, these results suggest that attentional lapse in association with EPP in the pgACC anticipates failure in response inhibition.

Keywords

Default-mode network (DMN); Attentional lapse; Event-related potential (ERP); Error preceding positivity (EPP); Stop-signal task

Introduction

Default mode network (DMN) regions demonstrate higher level of activation or functional connectivity during a resting state (Greicius et al., 2003, 2009; Greicius and Menon, 2004; Raichle et al., 2001), as well as self-referential processing, mentalizing and mind-wondering (Buckner and Carroll, 2007; Gusnard et al., 2001; Mason et al., 2007; Qin and Northoff, 2011), as compared to when individuals are engaged in goal-directed tasks (see Gusnard and

*Correspondence to: C.C. Chen, Center for Neurobiology and Cognitive Science, National Taiwan University, Taipei 106, Taiwan.
**Correspondence to: C.-S.R. Li, Department of Psychiatry, Yale University, New Haven, CT 06511, USA.

Raichle, 2001; Raichle and Snyder, 2007; Whitfield-Gabrieli and Ford, 2012 for review). Activation of the DMN also co-occurs with attentional lapses (Weissman et al., 2006) and precedes response errors (Eichele et al., 2008; Li et al., 2007). In our previous fMRI study of a stop-signal task (SST), perigenual anterior cingulate cortex (pgACC) showed greater activation in go trials preceding stop error than those preceding stop success trials (Li et al., 2007). In a flanker task, task-related areas decrease and DMN regions increase in activation before the occurrence of error (Eichele et al., 2008). These studies suggest that attentional lapses, or momentary disengagement from the external task, may disrupt goal-directed behaviors and cause response errors. In support of this hypothesis, other fMRI studies showed a negative correlation in activity between DMN and attentional control networks (Anderson et al., 2011; Fox et al., 2005; Fransson, 2005; Hellyer et al., 2014; Kelly et al., 2008). For instance, in a global/local selective attention task, the DMN increased in activation (or decreased in deactivation) in slow as compared to fast responses (Weissman et al., 2006).

Earlier event-related potential (ERP) studies showed an enhanced response-locked positivity – *error-preceding positivity* or EPP – at frontal locales in the trials preceding an error during cognitive control (Allain et al., 2004; Hajcak et al., 2005; Ridderinkhof et al., 2003). For instance, in a flanker task, the EPP occurred during correct responses preceding error trials as compared to those preceding correct trials (Ridderinkhof et al., 2003). Subsequent study replicated the EPP in flanker and Stroop tasks and further showed that the EPP did not occur in earlier trials or in trials following errors (Hajcak et al., 2005). It is suggested that the EPP might reflect a modulation of error-related or correct-response negativity potential generated from dorsal ACC (dACC) and disengagement of the monitoring system to detect subthreshold conflict or error response tendencies (Allain et al., 2004; Hajcak et al., 2005; Ridderinkhof et al., 2003). However, as there was no source reconstruction in these earlier ERP studies, the origin and psychological correlate of the EPP remain unclear.

We aimed to address this issue by identifying the source of EPP. A source in the pgACC supports attentional lapse prior to response errors. In contrast, a source in the dACC supports deficient conflict monitoring preceding response errors. We employed a stop signal task, in which participants responded to a go signal in most trials, and, in parallel, prepared to withhold the motor response when a stop signal appears (Chang et al., 2014; Li et al., 2007). With a staircase procedure to elicit errors in approximately half of the stop trials, we examined response-locked EPP and used source dipole modeling to locate its origin.

Methods

Participants

Twenty healthy adults (10 males, 22.4±1.3 years of age) participated in the study. The participants were all students of the National Taiwan University and naïve to the purposes of the experiment. All provided written consent and were financially compensated for their participation. The use of human participants followed the guideline of Helsinki Declaration and was approved by the Research Ethics Committee of National Taiwan University.

Behavioral task

The experimental design and procedures followed our previous work (Chang et al., 2014). We employed a simple reaction time (RT) task of the stop signal paradigm (Li et al., 2007; Verbruggen and Logan, 2009). There were two trial types, “go” and “stop,” randomly intermixed in presentation with a ratio of 3 to 1. The inter-trial interval was 2 s. A small white dot appeared at the center of a black screen to engage attention at the beginning of every trial. After an interval ranging randomly from 1 to 3 s (the “fore-period”), the dot turned into a circle (~2° of visual angle), which served as a “go” signal. The participants were instructed to quickly press a button at go signal onset but not before. The circle vanished either at button press or one second after go signal onset, whichever came first, and the trial was terminated. A premature button press before go signal onset also terminated the trial. In the stop trial, an additional “X”, or the “stop” signal, appeared and replaced the go signal. The participants were instructed to withhold button press upon seeing the stop signal. The trial terminated at the button press or one second after stop signal onset. The duration between go and stop signal onsets, or the stop-signal delay (SSD), was determined by a staircase procedure. The one-up-one-down procedure (Levitt, 1971) started with an SSD of 200 ms, and increased and decreased by 64 ms each after a successful and failed stop trial. By increasing and decreasing the SSD each following a stop success and error, the staircase procedure allows participants to succeed in approximately half of the stop trials.

The task was divided into 4 sessions, each with 100 trials and lasting no longer than 8 min, with a short break in between sessions. There were about 5 min of practice on the task prior to the experiments to ensure that they understood the task. Participants were instructed to “respond to the go signal quickly while watching out for the stop signal, which might appear occasionally” (Chang et al., 2014; Li et al., 2008).

Electroencephalography (EEG) acquisition

The EEG was collected with a whole-head, 256-channel geodesic EEG system with HydroCell Sensor Nets (Electrical Geodesics, Eugene, OR). This system provides uniform spatial sampling (~2 cm, sensor to sensor), covering the entire scalp surface and extending 120° in all directions from the vertex reference electrode. The EEG was amplified at a gain of 1000 and recorded with a vertex physical reference. Signals were digitized at 500 Hz with a 16-bit analog-to-digital converter, which allowed an amplitude resolution of 0.076 μV. The EEG was recorded with 0.01–100 Hz bandpass filter. The computer administering the task sent a digital trigger to the recording system at the onset of fixation and go signal of every trial.

Data preprocessing

The data were preprocessed by the following procedures off-line prior to statistical analysis. First, the raw data were filtered by a 1–100 Hz band-pass and a 60 Hz Notch (FIR) filter. Second, noisy channels, which contained more than 20% of samples exceeding a pre-designated threshold of 200 μV, were replaced by the average of the six nearest spatial neighbors. Typically, only two to four channels per session were substituted. Next, for each channel, the EEG epochs that contained a large percentage (15%) of data samples exceeding a threshold (40 μV)were excluded to remove artifacts related to eye blinks and/or

movements. An epoch was defined as the time window between −100 and 1000 ms of go signal onset in a trial for artifact detection. Once noisy channels were substituted and artifactual epochs were excluded, the EEG was re-referenced to the common average of all of the channels, and re-aligned to response-locked epoch defined as the time window between −200 and 500 ms of button-press onset. Baseline correction was performed by subtracting the mean voltage of a window from 100 to 0 ms before a reference time point (go signal onset) in each trial for each channel. All ERP waveforms were filtered by Butterworth third-order 40 Hz low-pass filter to eliminate high frequency noise for visualization and statistical analyses.

Source dipole modeling

Our sensor net provides a uniform spatial sampling (~2 cm, sensor to sensor), covering a scalp surface extended about 120° in all directions from the vertex reference electrode. Given that a cortex-to-scalp point spread function of about 2.5 cm (Gevins, 1990) is sufficient for precise topographical sampling (Slotnick, 2004), the data collected with our apparatus allowed us to make a precise source estimation.

We employed the brain electrical source analysis (BESA) software (version 6.0, BESA GmbH, Gräfelfing, Germany) to fit the equivalent current dipoles that generate the ERPs. BESA computes the forward solution of scalp distribution of electrical fields for the placed dipoles, and, through an iterative procedure with different dipole locations and orientations, identifies the best solution that matches the observed scalp distributions with minimum unexplained variance (residual variance or RV). Source dipole modeling was performed on the grand averaged response-locked epoch, across participants.

To minimize RV for source localization, we employed a genetic algorithm (number of populations: 5; population size: 1000; maximum of equal generations: 30) as implemented in BESA. Briefly, sets of parameters determining dipole location and orientation were generated as initial populations, followed by selection, crossover and mutation operations until the RV converged (Grech et al., 2008). The epochs were filtered by zero-phase 1 Hz high-pass (12 dB) and 40 Hz low-pass (24 dB) filters in BESA to remove DC shift and high frequency noise. We used the four-shell ellipsoidal model with BESA toolbox to solve the inverse problem. Although our head model was not MRI-based and represented a simplistic approximation to the realistic brain, empirical studies using electrodes implanted in the human brain to create artificial dipole sources showed that the four-shell head model localizes the source with approximately 1 cm of averaged errors (Cohen et al., 1990; Cuffin et al., 1991),which is reasonably accurate (see Slotnick, 2004 for a review). The locations of all 256 channels were provided by BSEA for the 256-channel HydroCel Geodesic Sensor Net. The locations of dipoles were presented in MNI coordinates.

Data analysis and statistics: error-preceding positivity

We first distinguished four main trial types: response (button press) in go trial (G), no response in go trial (F), stop success (SS), and stop error (SE). G trials were further divided into those that preceded an SS (pre-SS) and SE (pre-SE) trial. We obtained the contrast “pre-SE vs. pre-SS” trials for each individual participant to identify ERP preceding response

errors. We computed ERP components time locked to button press and corrected for a baseline 100 to 0 ms before response. The amplitude of the ERP component was computed from the ERP waveform averaged across trials for each participant, and the mean amplitude was taken for the predefined time window. We focused on Fz, Cz and Pz because these three channels were most sensitive to error-preceding ERP as reported previously (Ridderinkhof et al., 2003; Hajcak et al., 2005). The contrast ERP waveforms of individual participants were then used for random effects analysis (Penny and Holmes, 2004).

Pre-SE and pre-SS trials differed in RT (see section 'General behavioral performance'). While previous studies have demonstrated that the RT difference is unlikely to account for error-preceding ERPs (Hajcak et al., 2005; Ridderinkhof et al., 2003), we conducted a RT-matching analysis as employed in the earlier work to confirm that this was indeed the case. Briefly, our RT-matching algorithm selected the trials from different trial types with the most similar RT (Hajcak et al., 2005; Ridderinkhof et al., 2003). It began with either pre-SE or pre-SS trials, whichever had the smaller number of trial within each participant, and the trials were paired one by one to those of the other trial type with the closest RTs. The unpaired trials were excluded from analyses.

To assess the statistical difference between the ERP waveforms of different trials while controlling for multiple comparisons, we performed cluster-based analyses (Maris and Oostenveld, 2007) for each of the aforementioned statistical contrast. First, we used a moving time window of 50 ms with a 10 ms step, starting from response onset, and a paired *t*-test to examine the mean amplitude difference between ERP waveforms of each window. Second, we grouped the temporally adjacent windows with $p < 0.05$ (paired *t*-test) into single clusters. Third, we performed a paired *t*-test examine the difference in the mean amplitude for each cluster-based ERP waveform contrast. Finally, we applied Bonferroni correction to all identified clusters across the three channels to control for false positive rate of the cluster-based statistics.

Results

General behavioral performance

Subjects averaged with a go success rate of 97.8 ± 2.0% and RT of 399.3±61.9 ms. The rate of successful stop trials was 48.8±2.2% across subjects, suggesting the success of the staircase procedure in tracking participants' performance and eliciting errors in approximately half of the stop trials. The critical SSD was computed by a maximal likelihood procedure on the sequence of all staircase-generated SSDs for each participant, and the stop-signal reaction time (SSRT) was computed by subtracting the critical SSD from the median go RT for each participant, based on the race model (Li et al., 2008). The SSRT (217.1 ± 26.0 ms) was within the range reported in earlier studies. The reaction time (RT) of pre-SE (395.2 ± 60.9 ms, $n = 39.1 \pm 2.4$) was shorter than pre-SS (413.4 ± 69.1 ms, $n = 30.9 \pm 4.6$) trials ($p = 0.007$, paired *t*-test), replicating previous report that error-preceding go trials tend to have shorter RT than the correct-preceding go trials (Ridderinkhof et al., 2003).

Event-related potentials

We performed ERP analysis in the epochs response-locked to the button press for pre-SE and pre-SS trials.

To examine error-preceding ERPs (Fig. 1), we compared the waveforms of pre-SE and pre-SS trials first without RT matching. The cluster-based analysis identified three clusters at Cz and one cluster at Pz with mean amplitude of pre-SE > pre-SS. Among the four clusters, two at Cz met Bonferroni corrected threshold (n = 4, alpha = 0.013), each at 0–170 ms (2.42 ± 0.26 vs. 1.92 ± 0.31 μV, p = 0.006) and 260–450 ms (2.60 ± 0.76 vs. 1.98 ± 0.74, p = 0.004). The ERP cluster at 0–170 ms replicated EPP (time window 0–100 or 0–150 ms, response-locked) reported previously (Ridderinkhof et al., 2003; Hajcak et al., 2005). For convenience, we tentatively refer to the ERP at 260–450 ms as *late error-preceding positivity* (LEPP). Note that the statistical tests of the difference in EPP and LEPP amplitude were conducted on time points that were identified to differ between pre- SE and pre-SS trials. Thus, these analyses did not provide any new information but simply serve to provide a measure specific to the combined time points that defined EPP and LEPP.

The results of the analyses with pre-SE and pre-SS matched for RT were similar. Three clusters were identified and they all met Bonferroni corrected threshold (n = 3, alpha = 0.017): EPP at Cz at 0–150 ms (2.36 ± 0.29 vs. 1.90 ± 0.32, p = 0.007) and LEPP at Cz at 270–450 ms (2.46 ± 0.77 vs. 1.89 ± 0.73, p = 0.005) and at Pz at 400–490 ms (−2.82± 0.74 vs. −3.70 ± 0.89, p=0.014). Thus, confirming earlier work, EPP and LEPP were independent of RT difference between pre-SE and pre-SS trials.

The results on dipole sourcing reported in the below were based on analyses without matching for RT.

Source dipole localization

The source model of EPP (0–170 ms) was based on the response-locked waveform of pre-SE trials from 110 to 150 ms, where EPP showed the maximum amplitude at Cz. This also allowed us to avoid motor-related neural activities centered at 0 ms when participants made a response. The first component of principle component analysis (PCA) explained 98.4% of variance of the selected time window. A single-dipole source localization model showed a source at coordinates (3.3, 37.0, 2.6), in the area of pgACC, with the orientation (0.0, −1.0, 0.0), and the RV was 19.0%. The topographic map of EPP (110 to 150 ms) and the dipole model are shown in Fig. 2b.

The source model of LEPP (260–450 ms) was based on the response-locked waveform of pre-SE trials from 270 to 310 ms, where LEPP showed the maximum amplitude at Cz. The first component of PCA explained 99.8% of variance of the selected time window. A single-dipole model showed a source at coordinates (5.3, 27.6, −7.2), in the area of pgACC, with the orientation (0.0, 0.9, 0.5), and the RV was 12.0%. The topographic map of LEPP (270 to 310 ms) and location of the dipole are presented in Fig. 2b.

Given the spatial proximity of the dipole locations of EPP and LEPP, these two components might be generated by the same rather than two distinct sources. To test this possibility, we

fitted a single-dipole model to response-locked waveform of pre-SE trials over 110 to 310 ms. The first component of PCA explained 95.0% of variance of the selected time window. The source was at coordinates (4.8, 26.3, −7.7) with the orientation (0.0, 0.9, 0.4), and the residual variance was 15.4%.

Bootstrapping procedure for dipole fitting

To further confirm the origin of the dipole, we used a bootstrapping procedure to assess the statistical reliability of the location of fitted dipoles (Darvas et al., 2004, 2005). First, for each participant we resampled (with replacement) the pre-SE trials, with the number of resampled trials as in the original data. Second, the ERP epochs of the resampled pre-SE trials were averaged for each participant and then pooled across all the participants, generating one 256-channel bootstrapped ERP epoch for dipole fitting. Third, the previous two steps were repeated for 1000 times to obtain 1000 bootstrapped ERP epochs. Fourth, for each of the 1000 bootstrapped ERP epochs we employed the BESA to fit three types of dipoles: a free dipole (fit for both location and orientation), a dipole fixed at a coordinate for the pgACC (coordinates: 4, 32, 4; Li et al., 2007; fit for orientation only), and a dipole fixed at a coordinate for the dACC (coordinates: 0, 12, 49; van Veen, and Carter, 2002; fit for orientation only). When fitting a free dipole, we started with a regional source, which can be regarded as a source with three dipoles at the same location with orthogonal orientation, to obtain the best-fitted location, and then converted it into a dipole with best-fitted orientation. Therefore, we obtained 1000 sets of location and orientation from the fitted free dipoles and 1000 RVs from the dipole fitted at either pgACC or dACC.

For the EPP time window, the bootstrapped RV of the dipole fixed at pgACC was 20.74±2.44% (mean±standard deviation of bootstrapped sample) with 2.5% and 97.5% quantiles at 16.61% and 26.24%, and the bootstrapped RV generated by the dACC dipole was 41.69 ± 2.69% with 2.5% and 97.5% quantiles at 36.64% and 47.40%. For the LEPP time window, the bootstrapped RV of the dipole fixed at pgACC was 14.40 ± 0.96% with 2.5% and 97.5% quantiles at 12.57% and 16.52%, and the bootstrapped RV generated by the dACC was 33.59 ± 2.13% with 2.5% and 97.5% quantiles at 29.64% and 37.94%. The Wilcoxon signed rank test showed that the RV of the dipole fitted at pgACC was significantly smaller than the dipole fixed at dACC for both EPP ($p < 0.001$) and LEPP ($p < 0.001$). These results suggested that pgACC is indeed a statistical better fit as the source of EPP and LEPP.

Furthermore, we fitted the bootstrapped data with a free dipole without any location constraints. The bootstrapped free dipoles showed mean coordinates for EPP and LEPP each at (3.3, 36.8, 2.4) and (5.2, 27.6, −7.2) (Fig. 2b). The Mahalanobis distance, a statistic that describes the standardized Euclidean distance in the transformed space between a specified position and the mean of multivariate distributed data in the scale of covariance, between pgACC and the mean coordinates of the bootstrapped dipoles was 6.11 and 78.55 for EPP and LEPP, respectively. The Mahalanobis distances between dACC and the mean coordinates of the bootstrapped dipoles were 275.31 and 378.66 for EPP and LEPP, respectively. A shorter Mahalanobis distance represents a more reliable source of the observed ERP. Therefore, these results showed that the statistical location of dACC is

further from the bootstrapped center of free-fitted dipole locations than pgACC, suggesting that pgACC accounted for the source of both EPP and LEPP better than dACC.

Discussion

In this study, we employed the stop-signal task (SST) with the stop-signal delay varied in a staircase procedure to elicit errors in approximately half of the stop trials. We observed that the amplitude of error preceding positivity (EPP), including a component at 0–170 ms and a late component at 260–450 ms, was larger in the stop-error preceding go (pre-SE) trials, as compared to stop-success preceding go (pre-SS) trials. This result is consistent with the EPP reported in previous studies (Hajcak et al., 2005; Ridderinkhof et al., 2003).

Dipole source modeling shows that the EPP originates in the ventro-medial prefrontal cortex in the area of the perigenual anterior cingulate cortex (pgACC), a critical node of the default mode network (DMN). Thus, the EPP can be considered as a neural marker of attentional lapse in association with pgACC activation (Li et al., 2007). On the other hand, we did not find any evidence supporting the dorsal ACC (dACC) or supplementary motor area of the dorsomedial PFC, regions that are implicated in error monitoring, as the neural source of EPP (Allain et al., 2004; Hajcak et al., 2005; Ridderinkhof et al., 2003). Multiple lines of statistical analyses support the pgACC rather than dACC as the source of EPP.

In our analysis, we used a single-dipole model to estimate the location of the ERP source. Some may argue that there may be more than one source underlying our data. Indeed, the selection of the number of fitted dipole is one of the most contentious issues with source localization, because the operator and the number of fitted dipoles could influence the outcome. Thus, we fit a second dipole along with the first one. In all cases, the two-dipole model decreased RV no more than 4.6%. The location of the second dipole was either outside the brain or at an improbable location such as the lateral ventricle, suggesting that the second dipole mainly resulted from a fit to the noise. Hence, the single-dipole model is sufficient in identifying a common source of both EPP and LEPP in the area of pgACC. This result is consistent with our previous fMRI study (Li et al., 2007), employing an identical experimental design and statistical analysis and showing only one frontal region in relation to the current hypothesis, as well as our PCA result, as discussed above, showing that the first principal component explained up to 95% of the variance in all of the time windows examined.

Although the EPP/LEPP and error-related positivity (Pe) are both response-locked positive ERPs and share similar morphology, the evidence suggested that they are distinct ERP components. For instance, a study of the flanker task suggested that early Pe originates at dACC (equally fitted at (−3, −4, 29), (4, −4, 29) and (−3, −11, 29)) (Herrmann et al., 2004) or the left superior parietal cortex (−30, −22, 51) and late Pe originates at the frontal cortex (−12, 59, 22) (van Veen and Carter, 2002). Another EEG dipole modeling study employed difference waveform between correct and error response trials and showed that the Pe is generated in posterior cingulate regions (−0.7,−34.1, 35.6) (Vocat et al., 2008). On the other hand, the current dipole model showed that EPP and LEPP both originate in pgACC bordering on subgenual ACC. Furthermore, in a direct contrast, we showed that pgACC

outperformed dACC as the source of EPP and LEPP. Together with these earlier studies, our findings suggested that EPP/LEPP and Pe are distinct ERP components and support the hypothesis that attentional lapse rather than error monitoring associates with EPP. That is, activation of the pgACC, as part of the default mode network, is related to diminished mental engagement, which frequently precedes stop errors. More broadly, this contrasts with an account of the EPP/LEPP in terms of performance monitoring.

These findings are consistent with frequency spectrum analysis showing diminished theta band (4–8 Hz) power of the medial prefrontal cortex in the trials preceding errors in the flanker task (Cavanagh et al., 2009) and increased alpha band (8–14 Hz) power around 20 s prior to failure in target detection during a temporal attention task (O'Connell et al., 2009). Thus, moment-to-moment fluctuation in attention plays a preeminent role in determining cognitive performance and can be captured by EEG and fMRI.

These considerations have important implications for our understanding of the psychological processes that determine SST performance. In the studies of SST, many investigators compared brain activities between stop success (SS) and stop error (SE) trials to derive the neural correlates of motor response inhibition. That is, when inhibition is in place, participants are more likely to stop at the appearance of the stop signal. However, as we noted earlier, because attention is likely to fluctuate from one trial to the next, the extent to which participants are engaged in the task may determine trial outcome (Chao et al., 2009; Duann et al., 2009; Li et al., 2006). Indeed, the inferior frontal cortex, which responds to a contrast of stop versus go trials or SS versus SE trials, is a part of the ventral attention system (Cai et al., 2014; Corbetta and Shulman, 2011; Frank and Sabatinelli, 2012; Li et al., 2006). Thus, a direct contrast of SS and SE trials does not identify a “pure” construct of response inhibition. The current study examined whether attentional control or behavioral engagement earlier in time (“in the background”), before the stop signal appears, may also determine trial outcome. Thus, these ERP findings along with our previous fMRI work demonstrate a role of attention in determining cognitive performance, an issue of significance beyond the SST.

One question concerns whether other regions of the DMN, such as the precuneus, may also be involved and why the current study did not identify sources in these areas (Li et al., 2007; Zhang and Li, 2010, 2012). One possibility is the limitations of ERP techniques employed in the current study. For example, the ERP analysis may lack the sensitivity required in identifying and localizing sources that are deeper in the brain. This is an important issue that needs to be further explored in the future.

A recent study tested whether the EPP generalizes to behavioral tasks that involve minimal response conflict (Masaki et al., 2012). In an alternating-response task, participants responded to the pointing direction of an arrowhead, which alternated for 95% and repeated in the remaining 5% (lure) of the trials. The authors found no evidence that lure errors are foreshadowed by EPP and concluded that EPP is specific to behavioral tasks that involve response conflicts. On the other hand, the association between attentional lapse and DMN activity has been reported in many studies that do not explicitly require conflict control. Functional MRI showed anticorrelated activities between DMN and attentional control

network in individuals during resting state or performing attentionally demanding tasks (Anderson et al., 2011; Fox et al., 2005; Fransson, 2005; Hellyer et al., 2014; Kelly et al., 2008). During visual attention, Granger causality modeling showed that the task control network and DMN are anticorrelated in activity, and the activation level of DMN negatively correlated with behavioral performance (Wen et al., 2013). Indeed, in sensory discrimination, the difficulty of the task as determined by stimulus discriminability, short-term memory load and stimuli coherence level are all positively associated with higher deactivation level of DMN regions (McKiernan et al., 2003; Singh and Fawcett, 2008). Thus, activity of the DMN appears to impact behavioral outcome beyond cognitive control tasks, and one might be able to probe EPP in behavioral challenges as long as attention is demanded for optimal performance.

Conclusions

Error-preceding positivity potentials (EPP) are localized to the perigenual anterior cingulate cortex—a critical node of the default model network. While in the current study the EPP relates specifically to attentional lapse in the stop signal task, the finding may point to a general role of DMN activity in supporting cognitive performance, because of the omnipresence of attention in behavioral challenges. More broadly, ERP and fMRI studies of cognitive control have so far been conducted separately. By localizing an error-preceding ERP to the pgACC as guided by fMRI, the current study suggests the importance of combined EEG/fMRI studies in the future to examine and compare the electrical and BOLD correlates of many processes of importance to cognitive control.

Acknowledgments

This study was supported by Taiwan MOE 101R892101 (CCC), NIH grants DA023248, DA026990 (C-SRL) and AA021449 (C-SRL), and NSF grant BCS1309260 (C-SRL). The funders had no further role in study design; in the collection, analysis and interpretation of data; in the writing of the report; or in the decision to submit the paper for publication.

References

Allain S, Carbonnell L, Falkenstein M, Burle B, Vidal F. The modulation of the Ne-like wave on correct responses foreshadows errors. Neurosci. Lett. 2004; 372(1):161–166. [PubMed: 15531109]

Anderson JS, Ferguson MA, Lopez-Larson M, Yurgelun-Todd D. Connectivity gradients between the default mode and attention control networks. Brain Connect. 2011; 1(2):147–157. [PubMed: 22076305]

Buckner RL, Carroll DC. Self-projection and the brain. Trends Cogn. Sci. 2007; 11(2):49–57. [PubMed: 17188554]

Cai W, Ryali S, Chen T, Li CSR, Menon V. Dissociable roles of right inferior frontal cortex and anterior insula in inhibitory control: evidence from intrinsic and task-related functional parcellation, connectivity, and response profile analyses across multiple datasets. J. Neurosci. 2014; 34(44): 14652–14667. [PubMed: 25355218]

Cavanagh JF, Cohen MX, Allen JJ. Prelude to and resolution of an error: EEG phase synchrony reveals cognitive control dynamics during action monitoring. J. Neurosci. 2009; 29(1):98–105. [PubMed: 19129388]

Chang A, Chen CC, Li HH, Li CSR. Event-related potentials for post-error and post-conflict slowing. PLoS ONE. 2014; 9(6):e99909. [PubMed: 24932780]

Chao HH, Luo X, Chang JL, Li CSR. Activation of the pre-supplementary motor area but not inferior prefrontal cortex in association with short stop signal reaction time—an intra-subject analysis. BMC Neurosci. 2009; 10(1):75. [PubMed: 19602259]

Cohen D, Cuffin BN, Yunokuchi K, Maniewski R, Purcell C, Cosgrove GR, Schomer DL. MEG versus EEG localization test using implanted sources in the human brain. Ann. Neurol. 1990; 28(6): 811–817. [PubMed: 2285267]

Corbetta M, Shulman GL. Spatial neglect and attention networks. Annu. Rev. Neurosci. 2011; 34:569–599. [PubMed: 21692662]

Cuffin BN, Cohen D, Yunokuchi K, Maniewski R, Purcell C, Cosgrove GR, Schomer D. Tests of EEG localization accuracy using implanted sources in the human brain. Ann. Neurol. 1991; 29(2):132–138. [PubMed: 2012383]

Darvas F, Pantazis D, Kucukaltun-Yildirim E, Leahy RM. Mapping human brain function with MEG and EEG: methods and validation. NeuroImage. 2004; 23:S289–S299. [PubMed: 15501098]

Darvas F, Rautiainen M, Pantazis D, Baillet S, Benali H, Mosher JC, Leahy RM. Investigations of dipole localization accuracy in MEG using the bootstrap. NeuroImage. 2005; 25(2):355–368. [PubMed: 15784414]

Duann JR, Ide JS, Luo X, Li CSR. Functional connectivity delineates distinct roles of the inferior frontal cortex and presupplementary motor area in stop signal inhibition. J. Neurosci. 2009; 29(32):10171–10179. [PubMed: 19675251]

Eichele T, Debener S, Calhoun VD, Specht K, Engel AK, Hugdahl K, Ullsperger M. Prediction of human errors by maladaptive changes in event-related brain networks. Proc. Natl. Acad. Sci. 2008; 105(16):6173–6178. [PubMed: 18427123]

Fox MD, Snyder AZ, Vincent JL, Corbetta M, van Essen DC, Raichle ME. The human brain is intrinsically organized into dynamic, anticorrelated functional networks. Proc. Natl. Acad. Sci. 2005; 102(27):9673–9678. [PubMed: 15976020]

Frank DW, Sabatinelli D. Stimulus-driven reorienting in the ventral frontoparietal attention network: the role of emotional content. Front. Hum. Neurosci. 2012; 6:116. [PubMed: 22557960]

Fransson P. Spontaneous low-frequency BOLD signal fluctuations: an fMRI investigation of the resting-state default mode of brain function hypothesis. Hum. Brain Mapp. 2005; 26(1):15–29. [PubMed: 15852468]

Gevins, AS. Analysis of multiple lead data. In: Rohrbaugh, J.; Johnson, R.; Parasuraman, R., editors. Event-Related Potentials of the Brain. New York: Oxford University Press; 1990. p. 44-56.

Grech R, Cassar T, Muscat J, Camilleri KP, Fabri SG, Zervakis M, Xanthopoulos P, Sakkalis V, Vanrumste B. Review on solving the inverse problem in EEG source analysis. J. Neuroengineering Rehabil. 2008; 5(1):25.

Greicius MD, Menon V. Default-mode activity during a passive sensory task: uncoupled from deactivation but impacting activation. J. Cogn. Neurosci. 2004; 16(9):1484–1492. [PubMed: 15601513]

Greicius MD, Krasnow B, Reiss AL, Menon V. Functional connectivity in the resting brain: a network analysis of the default mode hypothesis. Proc. Natl. Acad. Sci. 2003; 100(1):253–258. [PubMed: 12506194]

Greicius MD, Supekar K, Menon V, Dougherty RF. Resting-state functional connectivity reflects structural connectivity in the default mode network. Cereb. Cortex. 2009; 19(1):72–78. [PubMed: 18403396]

Gusnard DA, Raichle ME. Searching for a baseline: functional imaging and the resting human brain. Nat. Rev. Neurosci. 2001; 2(10):685–694. [PubMed: 11584306]

Gusnard DA, Akbudak E, Shulman GL, Raichle ME. Medial prefrontal cortex and self-referential mental activity: relation to a default mode of brain function. Proc. Natl. Acad. Sci. 2001; 98(7): 4259–4264. [PubMed: 11259662]

Hajcak G, Nieuwenhuis S, Ridderinkhof KR, Simons RF. Error-preceding brain activity: robustness, temporal dynamics, and boundary conditions. Biol. Psychol. 2005; 70(2):67–78. [PubMed: 16168251]

Hellyer PJ, Shanahan M, Scott G, Wise RJ, Sharp DJ, Leech R. The control of global brain dynamics: opposing actions of frontoparietal control and default mode networks on attention. J. Neurosci. 2014; 34(2):451–461. [PubMed: 24403145]

Herrmann MJ, Römmler J, Ehlis AC, Heidrich A, Fallgatter AJ. Source localization (LORETA) of the error-related-negativity (ERN/Ne) and positivity (Pe). Cogn. Brain Res. 2004; 20(2):294–299.

Kelly AM, Uddin LQ, Biswal BB, Castellanos FX, Milham MP. Competition between functional brain networks mediates behavioral variability. NeuroImage. 2008; 39(1):527–537. [PubMed: 17919929]

Levitt H. Transformed up-down methods in psychoacoustics. J. Acoust. Soc. Am. 1971; 49(2B):467–477. [PubMed: 5541744]

Li CSR, Huang C, Constable RT, Sinha R. Imaging response inhibition in a stop-signal task: neural correlates independent of signal monitoring and post-response processing. J. Neurosci. 2006; 626(1):186–192. [PubMed: 16399686]

Li CSR, Yan P, Bergquist KL, Sinha R. Greater activation of the “default” brain regions predicts stop signal errors. NeuroImage. 2007; 38(3):640–648. [PubMed: 17884586]

Li CSR, Huang C, Yan P, Paliwal P, Constable RT, Sinha R. Neural correlates of post-error slowing during a stop signal task: a functional magnetic resonance imaging study. J. Cogn. Neurosci. 2008; 20(6):1021–1029. [PubMed: 18211230]

Maris E, Oostenveld R. Nonparametric statistical testing of EEG-and MEG-data. J. Neurosci. Methods. 2007; 164(1):177–190. [PubMed: 17517438]

Masaki H, Murphy TI, Kamijo K, Yamazaki K, Sommer W. Foreshadowing of performance accuracy by event-related potentials: evidence from a minimal-conflict task. PLoS One. 2012; 7(5):e38006. [PubMed: 22701541]

Mason MF, Norton MI, van Horn JD, Wegner DM, Grafton ST, Macrae CN. Wandering minds: the default network and stimulus-independent thought. Science. 2007; 315(5810):393–395. [PubMed: 17234951]

McKiernan KA, Kaufman JN, Kucera-Thompson J, Binder JR. A parametric manipulation of factors affecting task-induced deactivation in functional neuroimaging. J. Cogn. Neurosci. 2003; 15(3): 394–408. [PubMed: 12729491]

O'Connell RG, Dockree PM, Robertson IH, Bellgrove MA, Foxe JJ, Kelly SP. Uncovering the neural signature of lapsing attention: electrophysiological signals predict errors up to 20 s before they occur. J. Neurosci. 2009; 29(26):8604–8611. [PubMed: 19571151]

Penny, WD.; Holmes, AJ. Random-effects analysis. In: Frackowiak, R.; Friston, K.; Frith, C.; Dolan, R.; Price, C.; Zeki, S.; Ashburner, J.; Penny, WD., editors. Human Brain Function. Elsevier Press; 2004. p. 843-850.

Qin P, Northoff G. How is our self related to midline regions and the default-mode network? NeuroImage. 2011; 57(3):1221–1233. [PubMed: 21609772]

Raichle ME, Snyder AZ. A default mode of brain function: a brief history of an evolving idea. NeuroImage. 2007; 37(4):1083–1090. [PubMed: 17719799]

Raichle ME, MacLeod AM, Snyder AZ, Powers WJ, Gusnard DA, Shulman GL. A default mode of brain function. Proc. Natl. Acad. Sci. 2001; 98(2):676–682. [PubMed: 11209064]

Ridderinkhof KR, Nieuwenhuis S, Bashore TR. Errors are foreshadowed in brain potentials associated with action monitoring in cingulate cortex in humans. Neurosci. Lett. 2003; 348(1):1–4. [PubMed: 12893411]

Singh KD, Fawcett IP. Transient and linearly graded deactivation of the human default-mode network by a visual detection task. NeuroImage. 2008; 41(1):100–112. [PubMed: 18375149]

Slotnick, SD. Source localization of ERP generators. In: Todd, TC., editor. Event- Related Potentials: A Methods Handbook. Cambridge: MIT Press; 2004. p. 149-166.

van Veen V, Carter CS. The timing of action-monitoring processes in the anterior cingulate cortex. J. Cogn. Neurosci. 2002; 14(4):593–602. [PubMed: 12126500]

Verbruggen F, Logan GD. Models of response inhibition in the stop-signal and stop-change paradigms. Neurosci. Biobehav. Rev. 2009; 33(5):647–661. [PubMed: 18822313]

Vocat R, Pourtois G, Vuilleumier P. Unavoidable errors: a spatio-temporal analysis of time-course and neural sources of evoked potentials associated with error processing in a speeded task. Neuropsychologia. 2008; 46(10):2545–2555. [PubMed: 18533202]

Weissman DH, Roberts KC, Visscher KM, Woldorff MG. The neural bases of momentary lapses in attention. Nat. Neurosci. 2006; 9(7):971–978. [PubMed: 16767087]

Wen X, Liu Y, Yao L, Ding M. Top-down regulation of default mode activity in spatial visual attention. J. Neurosci. 2013; 33(15):6444–6453. [PubMed: 23575842]

Whitfield-Gabrieli S, Ford JM. Default mode network activity and connectivity in psychopathology. Annu. Rev. Clin. Psychol. 2012; 8:49–76. [PubMed: 22224834]

Zhang S, Li CSR. A neural measure of behavioral engagement: task-residual low-frequency blood oxygenation level-dependent activity in the precuneus. NeuroImage. 2010; 49(2):1911–1918. [PubMed: 19761851]

Zhang S, Li CSR. Task-related, low-frequency task-residual, and resting state activity in the default mode network brain regions. Front. Psychol. 2012; 3:172. [PubMed: 22661964]

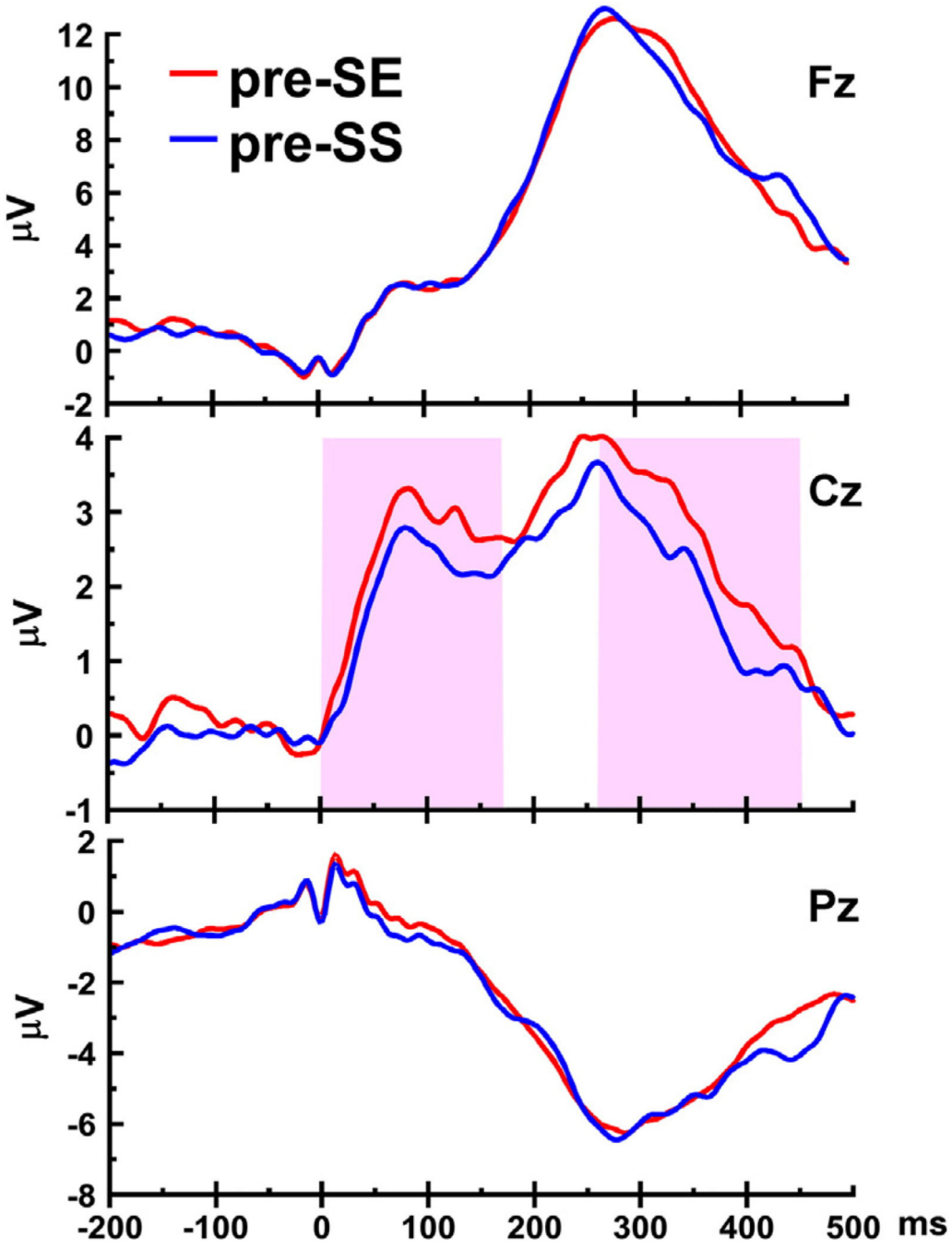

Fig. 1.

Response-locked ERP waveforms of pre-SE and pre-SS trials without RT matching at Fz, Cz and Pz channels. Time windows showing a significant difference in the mean amplitude between pre-SE and pre-SS waveforms are shaded in pink.

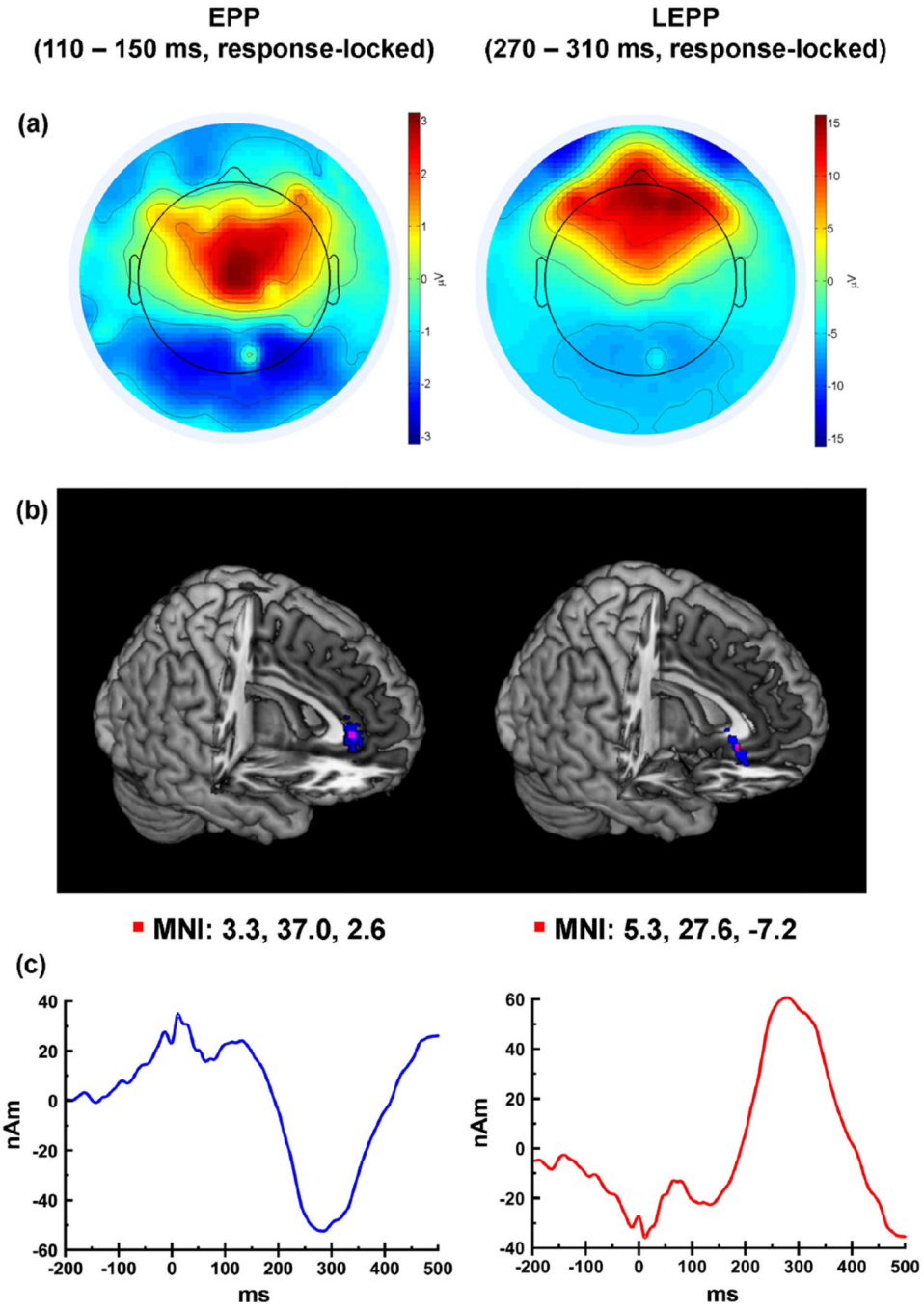

Fig. 2.

The topographic maps, locations of the dipoles, and the source waveforms of EPP (left panel) and LEPP (right panel) of grand averaged pre-SE trials across participants. (a) The topographic maps were based on the mean voltage of the specified time windows. (b) The red voxel represents the best-fitted dipole location of the observed data, and the blue area represents the distribution of 1000 bootstrapped dipole locations of each condition. The locations of the dipoles are distributed in the area of pgACC. Dipole locations are marked on a MNI template. (c) Source waveform was extracted from the best-fitted dipole of the

observed data of each condition. Two source waveforms are similar but with reverse polarities due to the opposite orientation of the dipoles.